Scientific Reports

https://doi.org/10.1038/s41598-026-55492-y

Article in Press

Fluorescent carbon dot-based biosensor for the rapid and sensitive detection of *Escherichia coli* DNA

Received: 12 January 2026

Accepted: 25 May 2026

Published online: 29 May 2026

Cite this article as: Hoang C.N.M., Nguyen S.H., Kraft M. *et al.* Fluorescent carbon dot-based biosensor for the rapid and sensitive detection of *Escherichia coli* DNA. *Sci Rep* (2026). https://doi.org/10.1038/s41598-026-55492-y

Chau Nguyen Minh Hoang, Son Hai Nguyen, Michael Kraft & Mai Thi Tran

Fluorescent Carbon Dot-Based Biosensor for the Rapid and Sensitive Detection of *Escherichia coli* DNA

Chau Nguyen Minh Hoang[1], Son Hai Nguyen[2*], Michael Kraft[3,4], Mai Thi Tran[1,5*]

[1] VinUni-Illinois Smart Health Center, VinUniversity, Hanoi, Vietnam

[2] School of Mechanical Engineering, Hanoi University of Science and Technology, Hanoi, Vietnam

[3] Micro- and Nanosystems (MNS), Department of Electrical Engineering (ESAT), KU Leuven, Leuven, 3000, Belgium

[4] Leuven Institute for Micro and Nanoscale Integration (LIMNI), Leuven, 3000, Belgium

[5] College of Engineering and Computer Science, VinUniversity, Hanoi, Vietnam

* Corresponding authors. E-mail: son.nguyenhai@hust.edu.vn and mai.tt@vinuni.edu.vn

Abstract

Rapid and accurate detection of pathogenic bacteria is critical for healthcare, food safety, and environmental monitoring. Here, we report a carbon dot-based fluorescent biosensor, prepared by a hydrothermal method, for sensitive and selective detection of *Escherichia coli* DNA. The carbon dots were characterized using field-emission scanning electron microscopy, X-ray diffraction, Fourier-transform infrared spectroscopy, and energy-dispersive X-ray spectroscopy, confirming their uniform nanoscale morphology, structural integrity, and surface functionality. An amino-modified NH_2-BL21 DNA probe enabled specific hybridization with the target sequence, producing quantifiable fluorescence changes. The biosensor exhibited a linear detection range of 50-250 fM, a limit of detection of 38.36 fM, recoveries of 87.06-113.57%, and stable performance over four weeks, with minimal cross-reactivity toward non-target sequences. Moreover, the carbon dot-based biosensor accurately detected *E. coli* DNA in drinking water and tap water, with recoveries of 95–126% and 93–119%, respectively, for concentrations of 75–225 fM. Lake water

recoveries ranged from 68–119% at low concentrations, indicating minor matrix effects. Unlike most previously reported carbon dot-based sensing strategies, which rely on enzymatic amplification or labeling, this work demonstrates an amplification-free and label-free fluorescence detection strategy that achieves femtomolar sensitivity through direct probe-target hybridization. The simple fabrication procedure, high repeatability, and robust analytical performance underscore the potential of this platform for the rapid, reliable, and cost-effective detection of *Escherichia coli* DNA. These findings highlight the promise of carbon dot-based fluorescent biosensors as practical tools for point-of-care diagnostics, environmental surveillance, and food safety monitoring.

Introduction

Escherichia coli (E. coli) is a facultative anaerobic, rod-shaped, gram-negative bacterium commonly found in the lower intestines of warm-blooded organisms[1]. While most *E. coli* strains are harmless and constitute a normal part of the gut microbiota, certain pathogenic variants, such as *enterohemorrhagic E. coli (EHEC), enteropathogenic E. coli (EPEC),* and *uropathogenic E. coli (UPEC)*, are responsible for a wide range of infections[2-4]. These infections range from foodborne illnesses and urinary tract infections to neonatal meningitis, as well as severe complications like hemolytic uremic syndrome[5]. Given its widespread prevalence and potential health risks, *E. coli* is widely recognized as a major biological contaminant in food products, drinking water, recreational water sources, and clinical environments[6,7]. Therefore, early and accurate detection of *E. coli* is crucial for preventing disease outbreaks, ensuring food safety, and maintaining water quality[8].

Traditional microbiological techniques, such as culturing on selective media, colony counting, and biochemical assays, remain the gold standard for detecting viable bacteria[9]. However, these methods are inherently time-consuming, typically requiring 24 to 72 hours for completion, and

often lack the sensitivity needed to detect low bacterial concentrations in complex matrices[10]. Moreover, they are unable to distinguish pathogenic from non-pathogenic strains without additional molecular analyses[11]. To address these limitations, DNA-based detection methods have been widely adopted. Molecular and immunological techniques, such as polymerase chain reaction (PCR), real-time PCR (qPCR), and loop-mediated isothermal amplification, enable highly specific detection by amplifying conserved genetic sequences unique to *E. coli*, while enzyme-linked immunosorbent assay detects the presence of bacterial antigens through antibody-based recognition[12-16]. These methods greatly enhance detection sensitivity and decrease false positives when compared to conventional culture-based techniques. Indeed, several PCR- and isothermal amplification-based commercial kits for *E. coli* DNA detection are currently available and widely used in food safety, clinical diagnostics, and environmental monitoring. However, their dependence on costly instruments, skilled personnel, and time-consuming protocols poses challenges for practicality in low-resource settings. Furthermore, the requirement for controlled laboratory conditions and intricate sample preparation diminishes their appropriateness for real-time, on-site, or field-deployable applications[17].

To address these practical limitations, biosensor-based detection platforms have attracted increasing attention as complementary analytical tools. A biosensor typically integrates a biological recognition element, such as DNA probes, antibodies, or enzymes, with a physicochemical transducer that converts the biorecognition event into a measurable optical, piezoelectrical, or electrochemical signal[18-22]. By enabling direct signal transduction from molecular recognition events, biosensors can offer simplified workflows, shorter analysis times, and potential compatibility with portable or field-deployable detection systems[23,24]. Among various biosensing modalities, fluorescence-based biosensors have attracted considerable attention

due to their high sensitivity, fast response, and compatibility with miniaturized detection systems[25,26]. These sensors are designed to detect subtle changes in fluorescence intensity or emission wavelength, which occur when specific molecular interactions, such as DNA hybridization or target binding, alter the fluorescent properties of a reporter molecule or nanomaterial.

In this context, carbon dot-based fluorescent nanomaterials have emerged as promising signal transducers for DNA biosensing because of their strong photoluminescence, excellent photostability, low cytotoxicity, and facile surface functionalization. In DNA detection systems, hybridization between a target sequence and a complementary probe can induce measurable fluorescence modulation of the nanomaterial, enabling quantitative detection[27-29]. Carbon dots (C-dots) are small quasi-spherical carbon nanoparticles with excellent optical properties and high aqueous stability[30,31]. Their surfaces contain abundant functional groups such as carboxyl, hydroxyl, and amino moieties, which facilitate straightforward functionalization with biomolecules, including DNA probes. Owing to these characteristics, C-dots have been widely explored as fluorescent transducers in biosensing platforms for pathogen detection and nucleic acid analysis[32,33].

Although carbon dot-based fluorescent probes have been previously investigated for bacterial sensing, the majority of reported studies emphasize whole-cell recognition mechanisms or depend on enzymatic amplification and fluorescence labeling strategies, which inherently increase system complexity and limit portability[34-36]. Direct, amplification-free detection of bacterial DNA using C-dots remains comparatively underexplored. In this context, the present study introduces a carbon dot-based fluorescent biosensing platform designed for direct nucleic acid recognition without the need for enzymatic amplification or secondary labeling. The C-dots were synthesized via a

hydrothermal route, producing fluorescent nanomaterials with abundant surface functional groups that facilitate stable probe immobilization and effective target interaction. Their physicochemical properties were systematically characterized using field-emission scanning electron microscopy (FE-SEM), X-ray diffraction (XRD), Fourier-transform infrared spectroscopy (FTIR), and energy-dispersive X-ray spectroscopy (EDX), ensuring structural integrity, chemical composition, and surface functionality relevant to biosensing performance.

The sensing capability of the developed platform was evaluated through fluorescence modulation induced by DNA hybridization, yielding a linear response over the femtomolar concentration range (50-250 fM) with a detection limit of 38.36 fM. Furthermore, the biosensor demonstrated reliable analytical performance, including high sequence selectivity, satisfactory recovery rates (87.06-113.57%), and stable signal output over a four-week storage period. To demonstrate practical applicability, the developed C-dot biosensor was evaluated in various environmental water matrices, including drinking water, lake water, and tap water. Recovery experiments using spiked DNA samples were conducted to assess the sensor's accuracy, matrix tolerance, and selectivity under realistic conditions. By leveraging the intrinsic optical properties and surface chemistry of C-dots, this platform offers a simplified yet sensitive alternative for DNA-based detection, with strong potential for translation into point-of-care diagnostics, environmental surveillance, and food safety monitoring.

Materials and Methods

Chemicals and Probes for *E. coli* DNA Detection

The following chemicals were utilized in this research: chitosan ($C_{56}H_{103}N_9O_{39}$, Shanghai Zhanyun Chemical Co., Ltd, Shanghai, China), thiourea (CH_4N_2S, 99%, Shanghai Macklin Biochemical Technology Co., Ltd., Shanghai, China), citric acid ($C_6H_8O_7$, 99.5%, Xilong Scientific Co., Ltd.,

China), and deionized water (DI). Chemicals used for extractions included Tris-HCl (Biobasic, Canada), Ethylenediaminetetraacetic acid (EDTA, Biobasic, Canada), Sodium chloride (NaCl, Merck, Germany), Sodium dodecyl sulfate (SDS, Xilong Scientific Co., Ltd., China) and Cetyltrimethylammonium bromide (CTAB, Biobasic, Canada). The oligonucleotide probe was designed to target *E. coli* DNA and utilized the sequence amine-5′ - CGGATGCGGCGTGAACGCCT 3′. All probes were synthesized by PHUSA Genomics Co., Ltd. (Can Tho, Vietnam), and the corresponding sequences are listed in Table 1.

Table 1. DNA probe sequences used in this study.

No	Probes	Sequence	Refs
1	NH_2-BL21	Amine-5'-CGGATGCGGCGTGAACGCCT-3'	37,38
2	Thiol-BL21	Thiol-5'-CGGATGCGGCGTGAACGCCT-3'	
3	No group-BL21	5'-CGGATGCGGCGTGAACGCCT-3'	
4	NH_2-membrane	Amine-5'-GCGGCCCTGGGTGGCATATTTATTGTCAGTGGTTTAATTCTGTTAATGAACTATAAC - 3'	39
5	NH_2-uidA	Amine-5'-TCG GCA TCC GGT CAG TGG CAG T-3'	40

Synthesis of Carbon Dots

The C-dots were synthesized by adapting the following procedure[41] (Fig. 1). 0.50 g of chitosan, 0.10 g of citric acid, and 0.50 g of thiourea were dissolved in deionized distilled water and allowed to stand at room temperature overnight with gentle stirring. The solution was then transferred to a Teflon-lined autoclave and heated to 200 °C for 6 hours. After this process, the resulting brown

solution was centrifuged at 6000 rpm for 45 minutes. Finally, the C-dots were collected from the supernatant and kept at 4 °C for future use.

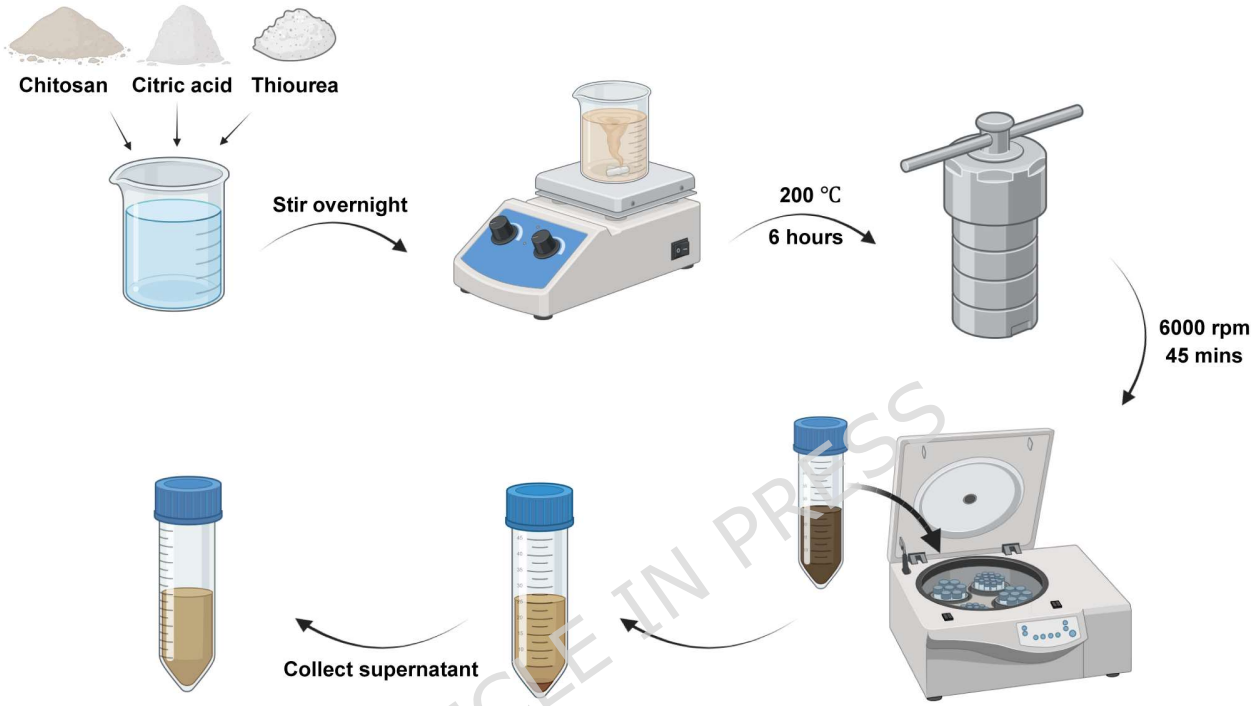

Figure 1. Schematic illustration of the hydrothermal synthesis of C-dots.

DNA Extraction Method

Four bacterial strains, *E. coli, Bacillus subtilis (B. subtilis), Enterococcus* spp., and *Vibrio proteolyticus (V. proteolyticus),* were obtained from the Microbiology and Genetics Laboratory at Hanoi University of Science and Technology in Hanoi, Vietnam. For DNA extraction, 1.5 mL of overnight bacterial culture was transferred to a 2.0 mL Eppendorf tube and centrifuged at 8,000 ×g for 5 minutes at room temperature using a Hettich MIKRO 200R centrifuge (Germany). The resulting pellet was resuspended in 740 µL of Tris-EDTA (TE) buffer.

Cell lysis was initiated by adding 20 µL of lysozyme (100 mg/mL), followed by incubation at 37 °C for 30 minutes in a dry bath incubator (Biologix Tekcovina, USA). Subsequently, 40 µL of

10% SDS and 8 µL of Proteinase K (10 mg/mL; Biobasic, Canada) were added to facilitate protein digestion and membrane disruption, and the mixture was incubated at 56 °C for 3 hours. To remove polysaccharides and other contaminants, 100 µL of 5 M NaCl and CTAB/NaCl (Merck, Germany) were gradually introduced, and the solution was heated at 65 °C for 10 minutes.

DNA was extracted using chloroform: isoamyl alcohol (Sigma-Aldrich) and centrifuged at 12,000 ×g for 10 minutes at room temperature. The aqueous phase containing the DNA was carefully transferred to a new tube. This extraction process was repeated until no visible white protein interface remained. DNA was precipitated with 100% ethanol (Merck, Germany) and either incubated at -20 °C for 2 hours or left overnight to enhance yield. The DNA pellet was collected by centrifugation at 12,000 ×g for 15 minutes at 4 °C, washed with 70% ethanol, air-dried, and finally resuspended in TE buffer (10 mM Tris-HCl, 1 mM EDTA, pH=8.0). The isolated DNA was stored at -20 °C for future use. All DNA samples exhibited OD260/280 ratios close to 2.0, indicating high purity suitable for downstream applications.

Fluorescent Measurement of *E. coli* DNA

For all measurements, the amino-modified probe was diluted to a final concentration of 30 nM in TE buffer. DNA solutions were prepared by dilution in 1×TE buffer (10 mM Tris-HCl, 1 mM EDTA, pH 8.0). DNA samples from *E. coli, V. proteolyticus, Enterococcus* spp., and *B. subtilis* were pretreated by heating at 98 °C for 10 minutes, followed by a 2-minute ice bath to prevent reannealing. A volume of 1000 µL of the C-dots was transferred to a 10 mm cuvette, with DI buffer used as the solvent. Next, 100 µL of the 30 nM probe solution was added to the mixture and incubated for 30 minutes at room temperature. Finally, 500 µL of DNA at different concentrations ranging from 50 to 250 fM was introduced. At each step, fluorescence measurements were recorded across the 460-600 nm wavelength range using a spectrophotometer (SpectraPro HRS-

300, Teledyne Princeton Instruments, Trenton, NJ 08619 USA) with a slit width of 400 μm. This procedure was performed at an excitation wavelength of 405 nm and an exposure time of 0.05 seconds. Each experiment was performed in three independent experiments, and within each experiment, three technical replicates were recorded, resulting in n = 9 measurements per group. Data are presented as mean ± standard deviation (SD). Statistical analysis was performed using one-way ANOVA followed by Dunnett's multiple comparison test.

Hybridization and fluorescence measurements were performed in deionized water at room temperature without added salts. The fluorescence signal became stable rapidly under the applied measurement conditions, and therefore detailed time-dependent kinetic analysis was not investigated in the present proof-of-concept study.

Results and Discussion

Characterization of Material

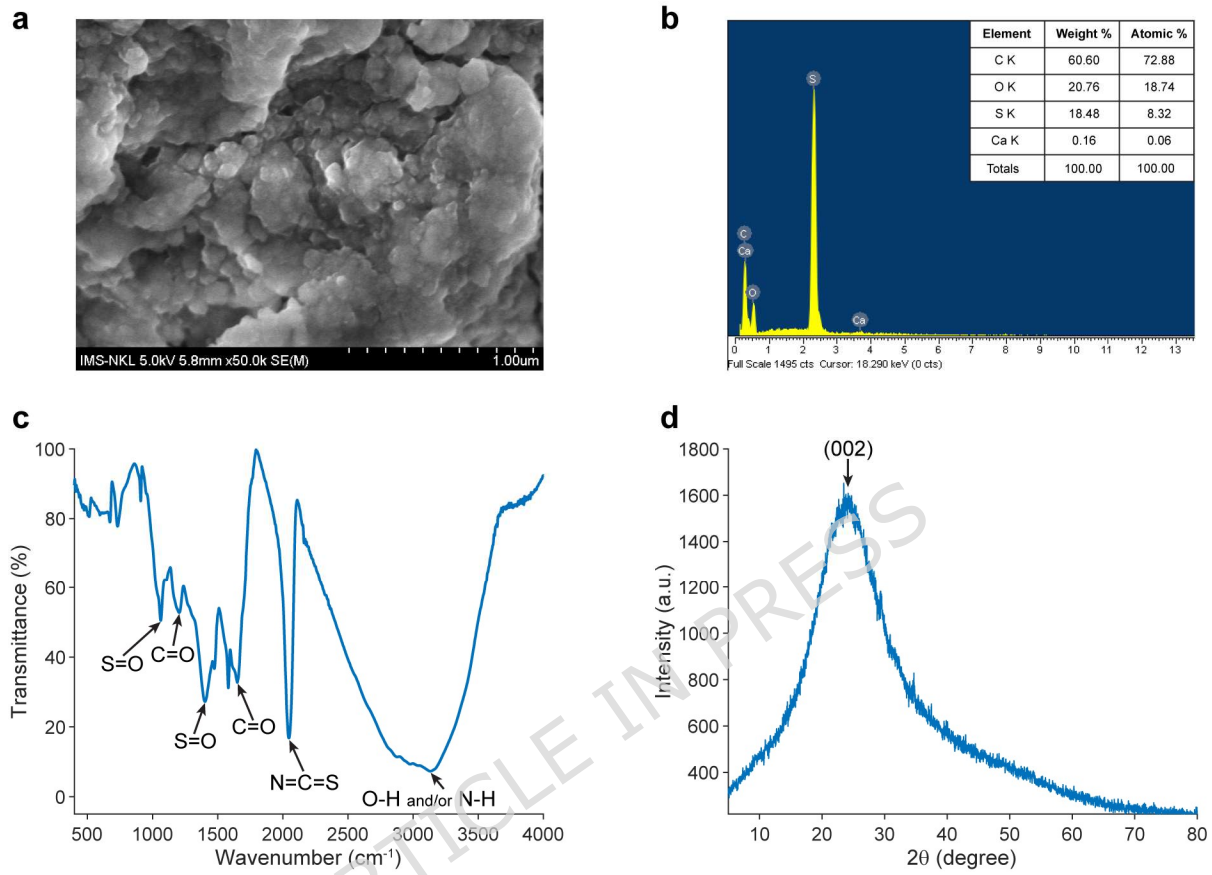

Figure 2. Structural and compositional characterization of C-dots: (**a**) FE-SEM image captured using a HITACHI-S4800; (**b**) EDX spectrum obtained from the same instrument (Hitachi High-Tech, Japan); (**c**) FTIR spectrum measured with a Jasco 4600 spectrometer (Jasco, Japan); (**d**) XRD pattern recorded with a Rigaku MiniFlex600.

The structural and physicochemical properties of the synthesized C-dots were examined using FE-SEM, EDX, FTIR spectroscopy, and XRD analysis, as illustrated in Fig. 2a-d. The FE-SEM image (Fig. 2a) reveals a clustered morphology consisting of aggregated nanoparticles with irregular surfaces. These aggregates form a porous network structure, suggesting a relatively high surface area that can facilitate interactions between the sensing interface and target DNA molecules.

The hydrodynamic size distribution of the synthesized C-dots was further analyzed using dynamic light scattering (DLS) with a Malvern Zetasizer Pro instrument (Malvern Panalytical, UK), as shown in Supplementary Fig. S1. The measurement yielded a Z-average hydrodynamic diameter of approximately 1087 nm, indicating the presence of hydrodynamic aggregates of carbon dots in aqueous suspension. This relatively large hydrodynamic size can be attributed to intermolecular interactions between surface functional groups (such as hydroxyl and carboxyl groups) that promote the formation of loosely associated clusters in solution. It should be noted that DLS measures the hydrodynamic diameter of particles in suspension, which includes the solvation layer and possible aggregates; therefore, the size obtained by DLS is typically larger than the core nanoparticle size observed by electron microscopy.

Energy-dispersive X-ray spectroscopy (Fig. 2b) further confirms the material's chemical composition. The EDX result shows a dominant presence of carbon (60.60 wt%) and oxygen (20.76 wt%), with notable amounts of sulfur (18.48 wt%), indicating the successful doping of heteroatoms during synthesis. Minor quantities of silicon and calcium were also detected, but their atomic percentages are negligible (<0.2%). Sulfur doping can play a vital role in tuning the electronic properties and enhancing the photoluminescent and stability properties of C-dots, thereby improving their performance in optoelectronic and catalytic applications[42-44]. This demonstrates the successful synthesis of C-dots and the doping of heteroatoms during the process.

The chemical functional groups on the surface of the C-dots were further investigated using Fourier transform infrared spectroscopy (Fig. 2c). The spectrum reveals multiple strong and broad peaks characteristic of both oxygen- and nitrogen-containing groups. The spectrum shows characteristic peaks corresponding to S=O (~1060 and ~1400 cm^{-1}), C=O (~1700 cm^{-1})[45,46]. Additionally, a smaller but distinct absorption around 2047 cm^{-1} is attributed to isothiocyanate

(N=C=S) stretching, further confirming the incorporation of nitrogen and sulfur-containing functionalities[47]. The broad and intense peak centered near 3400 cm^{-1} reflects the overlapping O-H and N-H stretching vibrations, suggesting the presence of hydroxyl and amine groups[47]. These surface functionalities enhance the C-dots' solubility in aqueous media and provide reactive sites for further functionalization or biomolecule conjugation.

X-ray diffraction analysis (Fig. 2d) was performed to examine the crystallinity of the material. A broad diffraction peak centered at approximately $2\theta = 24°$ is observed, which corresponds to the (002) plane of graphitic carbon, consistent with JCPDS reference card no-26-1076[48,49]. The broad nature of this peak suggests a low degree of structural order and limited graphitic stacking, a characteristic often observed in carbon-based nanomaterials, such as C-dots. In addition to intrinsic disorder, the peak broadening may be attributed to extensive surface functionalization. The presence of oxygen-containing groups (e.g., hydroxyl, carboxyl, or epoxy) disrupts π-π stacking between graphitic layers, resulting in increased interlayer spacing and turbostratic disorder[50,51].

Overall, the combined FE-SEM, EDX, FTIR, and XRD results confirm the successful synthesis of heteroatom-doped C-dots with abundant surface functionalities, an amorphous graphitic structure, and a chemical composition well suited for sensing applications.

Fluorescence Biosensor for Detecting *E. coli* DNA

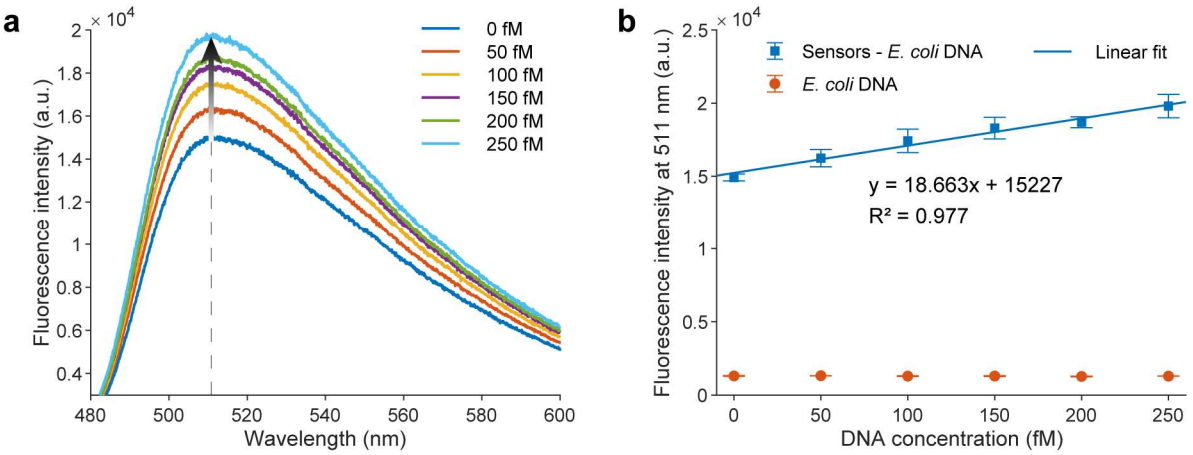

Figure 3. The fluorescence spectra of the hybridization of C-dots solution with (**a**) Probes and various concentrations of *E. coli* DNA, ranging from 0 to 250 fM, and (**b**) A linear relationship exists between DNA concentration and fluorescence values over the concentration range of 50-250 fM, measured at a wavelength of 511 nm.

To evaluate the performance of the fluorescence-based biosensor for *E. coli* DNA detection, fluorescence emission spectra were recorded over a wavelength range of 480-600 nm. Different concentrations of target DNA were introduced to the biosensors to facilitate hybridization between the probe and target DNA strands. This specific binding event resulted in measurable changes in fluorescence intensity, which served as the analytical signal for DNA detection. To validate sensor selectivity, *E. coli* DNA was used as a positive control, while non-target DNAs from *B. subtilis, V. proteolyticus*, and *Enterococcus* spp. served as negative controls, which produced negligible fluorescence changes, confirming the high specificity of the biosensor. Upon increasing *E. coli* DNA concentrations from 0 to 250 fM, a systematic enhancement in fluorescence emission was observed, particularly at the emission wavelength of 511 nm (Fig. 3a). This enhancement is attributed to alterations in the local electronic environment of the fluorophore, induced by hybridization with *E. coli* DNA and the probe[20]. Quantitative analysis was performed by plotting the fluorescence intensity at 511 nm against the target DNA concentration over the range of 50 to

250 fM (Supplementary Fig. S2). The corresponding raw fluorescence data used for calibration and LOD calculation are summarized in Supplementary Table S1. As shown in Fig. 3b, the calibration curve exhibited good linearity and was described by the equation:

$$y = 18.663x + 15227, \quad (1)$$

where y represents the fluorescence intensity at 511 nm and x denotes the DNA concentration (fM). The high correlation coefficient ($R^2 = 0.977$) indicates the strong linear relationship between fluorescence response and analyte concentration, which is critical for reliable quantitative analysis. The limit of detection (LOD) was calculated using the formula LOD = 3σ/S, where σ is the standard deviation, and S represents the coefficient of the x-variable. The LOD was determined to be 38.36 fM, demonstrating the sensor's ability to detect ultralow concentrations of target DNA with high sensitivity.

To evaluate the accuracy and practical applicability of the biosensor, recovery experiments were performed by spiking known concentrations of *E. coli* DNA (75, 125, and 225 fM) into the sensing system. Using Eq. (1), the concentrations estimated from fluorescence measurements were 75.03, 108.82, and 252.80 fM, respectively (Table 2). The corresponding recovery rates ranged from 87.06% to 113.57%, indicating good agreement between the spiked and measured values. In addition, the relative standard deviation (RSD) values were low (1.56%-2.39%), indicating good precision and reproducibility of the method.

Table 2. Random samples used for model validation.

Spiked concentration (fM)	Measured fluorescence intensity at 511 nm (a.u.)	Estimated concentration (fM)	Recovery (%)	RSD
75	16627	75.03	100.02	1.564
125	17258	108.82	87.06	2.39
225	19945	252.8	112.35	1.73

These results demonstrate that the developed biosensor provides accurate and reliable DNA quantification at low concentration levels. Overall, the combination of robust fluorescence signal enhancement, a low detection limit, a wide linear dynamic range, and high recovery rates indicates that this sensing platform is a reliable tool for detecting trace levels of *E. coli* DNA.

As depicted in Fig. 4, the detection of *E. coli* is based on hybridization between the target DNA and carbon dot-DNA probe conjugates. Prior FTIR analysis confirmed that these C-dots possess a high density of carboxyl (-COOH) groups, which serve as vital binding sites for the amine ($-NH_2$) groups of the modified DNA probes (Fig. 2d). Immobilization occurs primarily via electrostatic interactions between the -COOH and $-NH_2$ groups, establishing a stable sensing interface. This strategic attachment ensures that the probe strands are optimally oriented and accessible on the surface, significantly enhancing specificity for recognizing complementary DNA sequences.

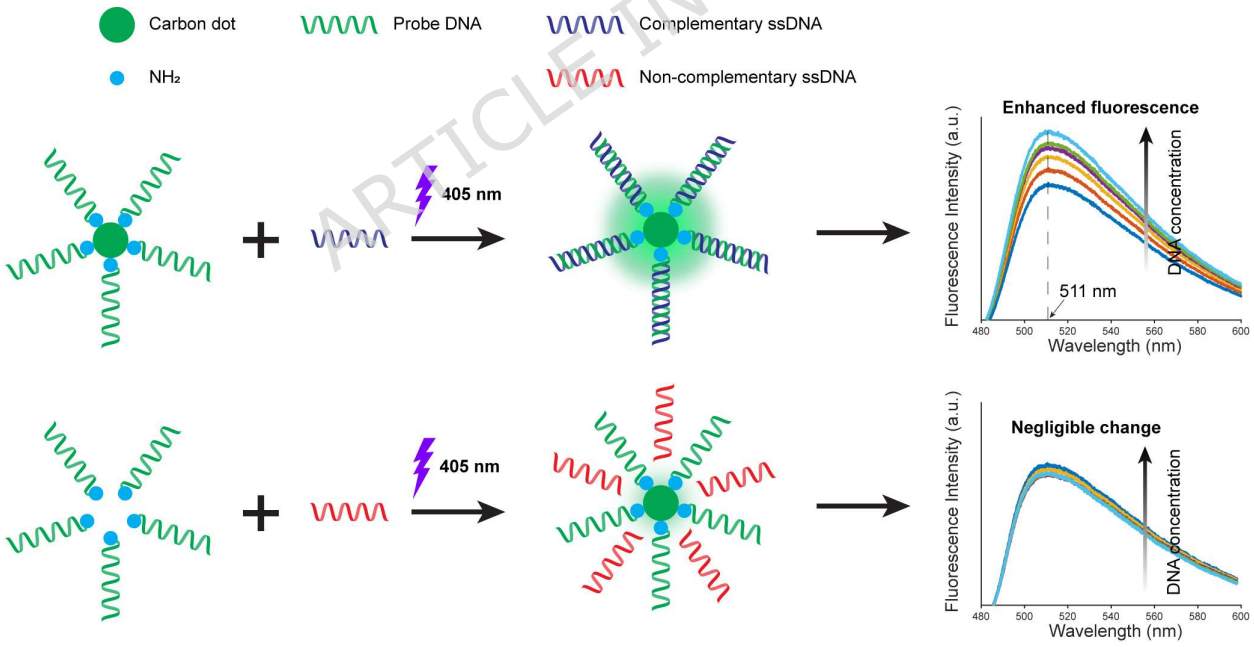

Figure 4. Schematic illustration of the DNA detection mechanism for *E. coli*.

The single-stranded DNA (ssDNA) alone exhibits negligible fluorescence over the concentration range of 50-250 fM (Supplementary Fig. S3). Upon the introduction of complementary *E. coli*

ssDNA (5'-AGGCGTTCACGCCGCATCCG-3'), hybridization occurs with the immobilized probes, resulting in the formation of double-stranded DNA (dsDNA) on the surface of the C-dots. This process alters the local physicochemical environment by reorganizing the hydration layer, modifying dielectric properties, and affecting base-stacking interactions[52]. These changes result in a substantial enhancement of the photophysical properties of the C-dots, manifesting as a notable increase in fluorescence intensity at 511 nm. The fluorescence response increases proportionally with the concentration of complementary DNA, enabling sensitive and quantitative detection. In contrast, non-complementary ssDNA (5'-TTATTATAAGTATTATTATT-3') induces negligible changes at 511 nm, indicating the absence of hybridization and minimal perturbation of the surface environment. This clear distinction between complementary and non-complementary responses demonstrates that specific probe-target hybridization selectively activates the sensing mechanism. Because the sensing mechanism relies on Watson-Crick base pairing, mismatched or non-complementary sequences are thermodynamically unfavorable to hybridize with the immobilized probe under the experimental conditions, thereby minimizing nonspecific signal generation. To further support the sequence selectivity of the sensing platform, the sequences of the control ssDNA strands were provided, and BLAST analysis was performed to verify the probe's specificity for the target *E. coli* DNA. The representative alignment results are summarized in Supplementary Table S2.

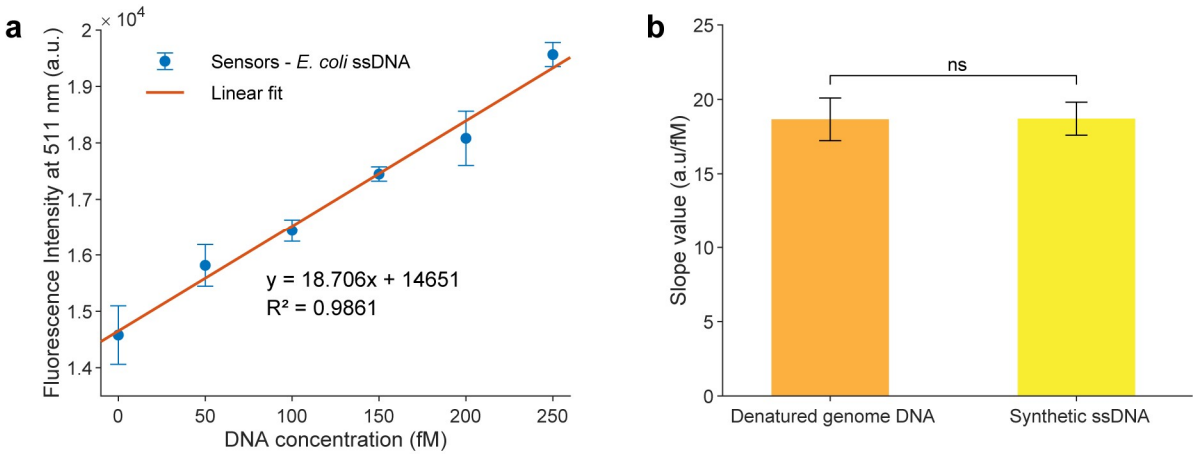

Figure 5. Validation of the carbon dot-based sensor using synthetic *E. coli* DNA: (**a**) Fluorescence response at 511 nm as a function of synthetic ssDNA concentration, showing a linear relationship (R^2 = 0.9861); (**b**) Comparison of calibration slopes obtained from denatured genomic DNA and synthetic ssDNA, indicating no statistically significant difference (ns).

To further validate the detection mechanism, synthetic ssDNA sequences complementary to the probe were evaluated under identical conditions. As demonstrated in Fig. 5a, the fluorescence intensity at 511 nm increased proportionally with the concentration of synthetic DNA, revealing a strong linear correlation (R^2 = 0.9861). This linear response reinforces the notion that the observed photoluminescence enhancement is a direct result of probe-target hybridization, rather than nonspecific interactions or background noise. Notably, the slope of the calibration curve for synthetic ssDNA (18.706 a.u./fM) closely matches that for *E. coli* DNA (18.663 a.u./fM), with no statistically significant difference identified (Fig. 5b).

These results suggest that the fluorescence response is driven solely by localized hybridization with the complementary sequence, remaining unaffected by variations in DNA strand length or complexity. Both full-length *E. coli* DNA and shorter synthetic targets induce comparable physicochemical changes at the carbon dot interface, reinforcing the underlying mechanistic rationale. Collectively, these findings provide evidence that NH_2-modified probes bind effectively to -COOH-functionalized C-dots, and that subsequent hybridization with complementary DNA

consistently enhances fluorescence at 511 nm. This validation underscores the specificity, reliability, and robustness of the proposed biosensing strategy for *E. coli* detection.

Selectivity of the Proposed Sensors

The selectivity of the developed fluorescence-based biosensor for *E. coli* DNA was evaluated by comparing its response to non-target bacterial DNAs, including *V. proteolyticus, B. subtilis*, and *Enterococcus* spp. (Supplementary Fig. S4). The DNA probe used in this study was designed based on previously reported *E. coli*-specific gene regions, enabling selective recognition of the target sequence [37,38]. As shown in Fig. 6a, incubating with increasing concentrations of *E. coli* DNA (ranging from 0 to 250 fM) resulted in a significant increase in fluorescence intensity at 511 nm, indicating successful hybridization between the probe and its complementary target DNA sequence. In contrast, the fluorescence responses to non-target bacterial DNA samples remained close to baseline levels under identical conditions, demonstrating high sequence discrimination and minimal cross-reactivity.

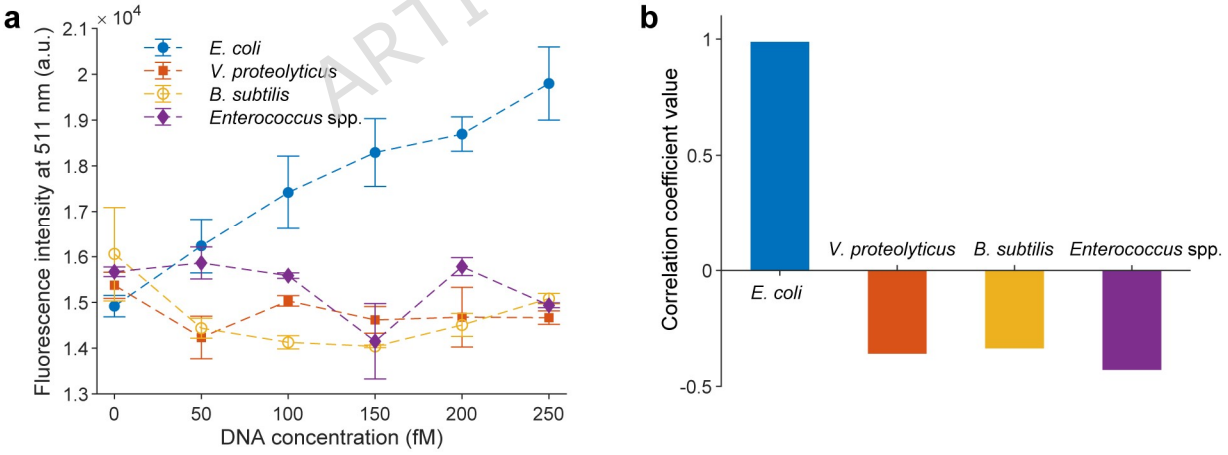

Figure 6. Selectivity analysis of the DNA biosensor toward *E. coli* DNA: (**a**) Fluorescence response at 511 nm to varying concentrations (0-250 fM) of *E. coli, V. proteolyticus, B. subtilis*, and *Enterococcus* spp. DNA; (**b**) Corresponding linear correlation coefficients obtained from fluorescence intensity versus DNA concentration for each bacterial species, showing significantly higher correlation for *E. coli* DNA.

To further quantify these differences, linear correlation coefficients between fluorescence intensity and DNA concentration were calculated for each bacterial DNA sample, with the corresponding comparisons shown in Fig. 6b. The sensor response to *E. coli* DNA exhibited a strong positive linear relationship, with a correlation coefficient close to unity, indicating high consistency and predictability of the fluorescence signal. In contrast, DNA from *V. proteolyticus*, *B. subtilis*, and *Enterococcus* spp. produced small negative correlation coefficients, reflecting a weak and non-systematic relationship between fluorescence intensity and DNA concentration. These results confirm the absence of significant probe-target hybridization with non-target DNA sequences. These findings indicate that the designed probe exhibits high binding affinity and sequence complementarity toward *E. coli* DNA, which is essential for accurate detection in complex biological samples. Overall, the sensor demonstrates high specificity for *E. coli* DNA, supporting its potential application in highly selective microbial diagnostic platforms.

Stability of the Proposed Sensors

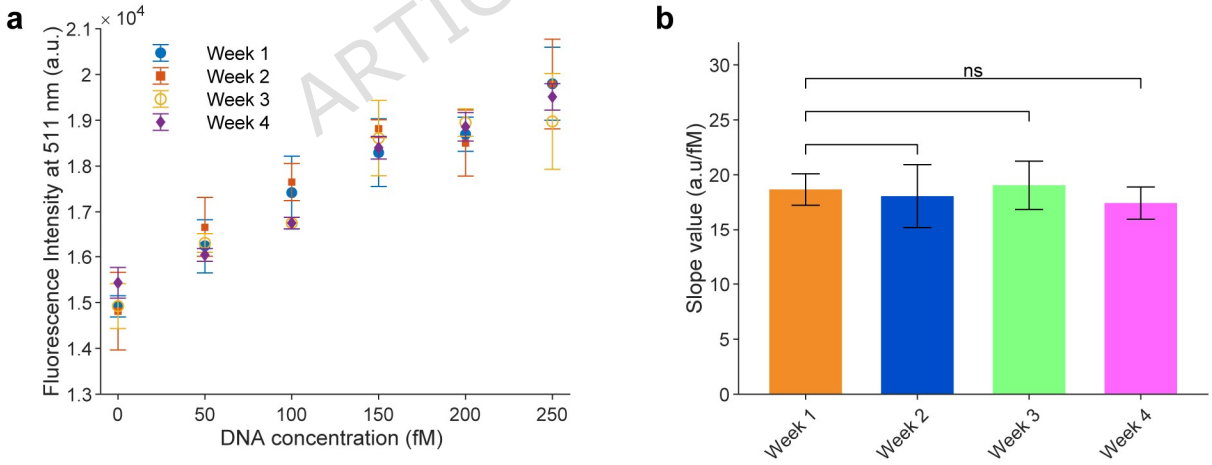

Figure 7. Stability assessment of the fluorescence-based *E. coli* DNA sensor over 4 weeks: (**a**) Fluorescence intensity at 511 nm as a function of DNA concentration (0-250 fM) measured at weekly intervals (Week 1-Week 4); (**b**) Comparison of slope values derived from the calibration curves at each time point, showing no statistically significant difference (ns) over time. Data are expressed as mean ± SD from three biological replicates, each measured in triplicate (n = 9).

Statistical analysis was performed using one-way ANOVA followed by Dunnett's multiple comparison test.

The storage stability of the fluorescence-based biosensor for *E. coli* DNA detection was evaluated over a four-week period. The sensor was stored at 4 °C and tested weekly to assess changes in performance over time. Fluorescence measurements were performed by incubating the sensor with *E. coli* DNA at concentrations ranging from 0 to 250 fM and recording photoluminescence intensity at 511 nm (Fig. 7a). At each time point, the fluorescence signal increased proportionally with DNA concentration, consistent with the hybridization-based sensing mechanism.

The biosensor exhibited a linear relationship between fluorescence intensity and DNA concentration throughout the storage period, with consistently high correlation coefficients (R^2), indicating preserved linearity. The corresponding linear regression equations and R^2 values are summarized in Table 3.

Table 3. Linear regression equations and R^2 values of the *E. coli* DNA sensor over 4 weeks of storage.

	Linear equation	**R^2**
Week 1	y = 18.663x + 15227	0.977
Week 2	y = 18.06x + 15449	0.91
Week 3	y = 19.055x + 14972	0.95
Week 4	y = 17.435x + 15319	0.97

At Week 1, the calibration curve was described by y = 18.663x + 15,227 (R^2 = 0.977). After one week of storage, the slope decreased slightly to 18.06 (R^2 = 0.91). In Week 3, the slope increased to 19.055 with an R^2 of 0.95, followed by a slope of 17.435 at Week 4 (R^2 = 0.97). These variations

indicate minor fluctuations in signal amplification during storage; however, the consistently high R^2 values confirm that the sensor retained reliable linear responsiveness throughout the four-week period.

To statistically evaluate these variations, calibration slopes from all time points (Weeks 1-4) were compared using one-way ANOVA (Fig. 7b). One-way ANOVA showed no significant difference among the four weeks ($F(3, 32) = 1.052$, $p = 0.3832$), indicating that the signal remained stable over time. Post hoc Dunnett's multiple-comparison test showed that none of the weeks differed significantly from Week 1 (all $p > 0.05$). Overall, these results demonstrate that the biosensor maintains good storage stability under refrigerated conditions, with minimal performance degradation. The sustained linear response and statistically consistent sensitivity highlight the sensor's robustness and reliability for prolonged nucleic acid detection.

Real Sample Validation in Environmental Water Matrices

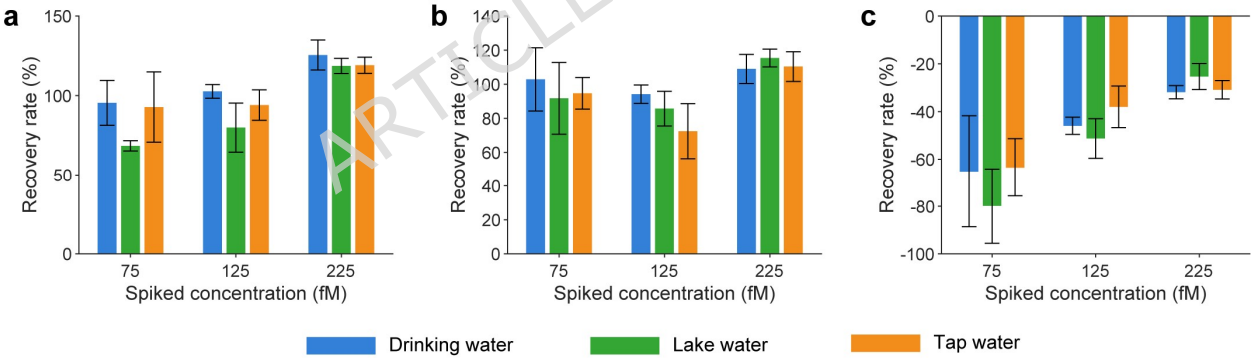

Figure 8. Recovery performance of the C-dot biosensor for *E. coli* DNA detection in environmental water matrices. Recovery rates obtained from drinking water, lake water, and tap water samples spiked with nucleic acid targets at concentrations of 75–225 fM. (**a**) Genome ssDNA (*E. coli*), (**b**) synthetic ssDNA (Complementary), and (**c**) synthetic ssDNA (Non-complementary), which served as a control to assess the selectivity of the biosensor.

Following the stability evaluation described in the previous section, which confirmed that the C-dot biosensor maintained consistent fluorescence responses and sensitivity over a four-week

storage period, the practical applicability of the sensing platform was further assessed using real environmental water matrices. Recovery experiments were performed in three representative water samples, drinking water, lake water, and tap water, to evaluate the analytical accuracy and selectivity of the proposed biosensor under realistic conditions (Supplementary Table S3).

As shown in Fig. 8a, the genome ssDNA of *E. coli* spiked into the different water matrices was successfully detected by the developed sensor across the tested concentration range (75–225 fM). In drinking water, recovery values ranged from 95.5% to 125.5%, while tap water samples exhibited recoveries between 92.8% and 119.1%, indicating good analytical accuracy in relatively clean matrices. In lake water, recoveries varied from 68.5% to 118.6%, with slightly lower values observed at lower concentrations. This deviation can be attributed to the presence of natural organic matter and dissolved ions in environmental water, which may partially influence fluorescence responses or probe–target hybridization efficiency. Nevertheless, the overall recovery range remained within acceptable limits for trace-level nucleic acid detection, demonstrating that the biosensor retains reliable performance even in complex aqueous environments.

To further evaluate the hybridization-based sensing mechanism, synthetic complementary ssDNA sequences were tested under identical conditions (Fig. 8b). The obtained recoveries remained consistently high across all matrices, ranging from 94.2% to 109.0% in drinking water, 85.7% to 115.4% in lake water, and 72.5% to 111.9% in tap water. The similarity between the recovery trends of genomic and complementary synthetic DNA confirms that the fluorescence response of the biosensor originates from specific probe–target hybridization rather than matrix-dependent artifacts.

Selectivity of the sensing platform in real matrices was further examined using synthetic non-complementary ssDNA as a control target (Fig. 8c). In contrast to the complementary sequences,

the non-complementary DNA produced negligible or negative recovery values across most tested concentrations, indicating the absence of significant nonspecific interactions between the probe-functionalized C-dots and unrelated nucleic acid sequences. These results confirm that the fluorescence signal modulation is primarily governed by sequence-specific hybridization events.

Overall, the recovery experiments demonstrate that the proposed C-dot biosensor maintains both high analytical accuracy and strong sequence selectivity in various environmental water matrices. The ability to reliably quantify femtomolar concentrations of *E. coli* DNA in complex aqueous environments highlights the robustness of the sensing platform and underscores its potential for practical applications in environmental monitoring, water quality assessment, and rapid pathogen detection in real-world samples.

Optimization of DNA Probes for Enhanced Sensing Using Carbon Dots

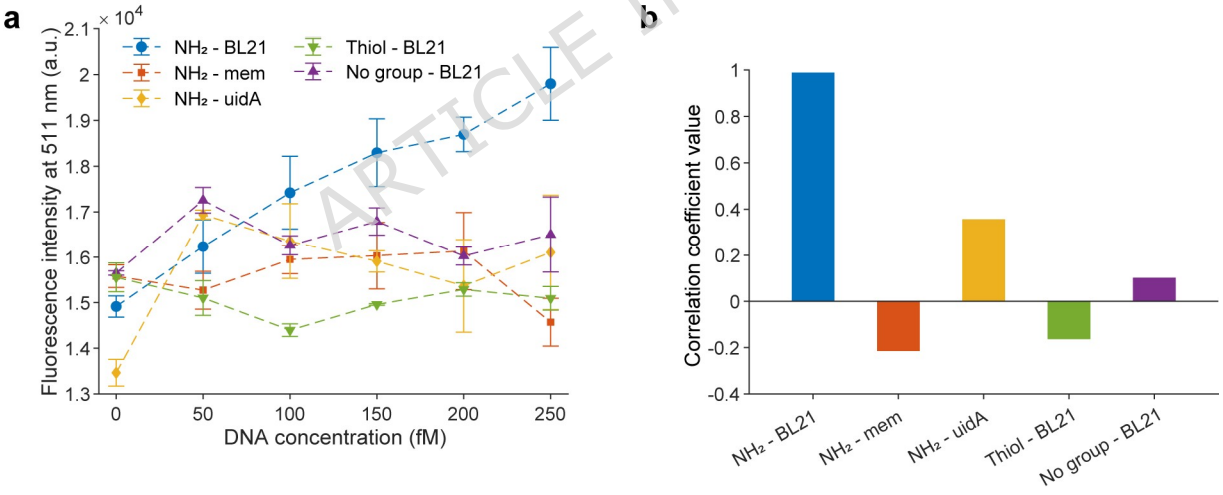

Figure 9. Effect of probe modification on the performance of the *E. coli* DNA sensor: (**a**) Fluorescence intensity response of the biosensor using different DNA probes (NH_2-BL21, NH_2-mem, NH_2-uidA, No group-BL21, and Thiol-BL21) across increasing *E. coli* DNA concentrations (0-250 fM); (**b**) Comparison of linear correlation coefficients obtained from fluorescence intensity versus DNA concentration for different probes.

The performance of the *E. coli* DNA sensor was significantly influenced by the selection and modification of DNA probes, as demonstrated by fluorescence intensity responses of the biosensor (Supplementary Fig. S5). In addition to probe optimization, this comparison also provides insight into the interaction between the DNA probes and the carbon dot surface. As shown in Fig. 9, NH_2-BL21 probe exhibited the highest sensing performance among all probes evaluated. Fluorescence intensity of NH_2-BL21 displayed a steep calibration slope with a strong correlation to DNA concentration, whereas the responses of other probes fluctuated around the mean value and showed weak relationships with DNA concentration.

Evaluation of BL21 probe variants revealed distinct differences associated with their terminal functional groups. In particular, the NH_2-BL21 probe demonstrated a strong concentration-dependent fluorescence response. In contrast, the Thiol-BL21 and No group-BL21 probes exhibited weak correlations with DNA concentration, indicating poor signal stability (Fig. 9b). This clear dependence of sensing performance on probe terminal functionalization suggests that amino groups facilitate more effective interaction and immobilization of the probe on the carbon dot surface.

Further comparison of probes sharing the same amino functional group but differing in nucleotide sequence revealed additional variability. While the NH_2-BL21 probe maintained a strong linear response, the NH_2-uidA probe showed only moderate correlation (linear correlation coefficient ≈ 0.4), and the NH_2-mem probe exhibited a weak negative correlation. These findings indicate that, once stable immobilization is achieved through NH_2 functionalization, hybridization efficiency, governed by sequence complementarity and target accessibility, becomes the dominant factor influencing sensor performance.

Overall, these results reinforce the importance of amino functionalization for stable and effective probe anchoring, while highlighting that sequence-dependent hybridization efficiency ultimately determines sensor performance. Therefore, the probe comparison experiments in Fig. 9 not only identify the optimal probe design but also provide functional evidence supporting the interaction between the amino-modified DNA probe and the carbon dot surface. Among all probes tested, the NH_2-BL21 probe exhibited the highest sensitivity, best reproducibility, and most reliable linear response for *E. coli* DNA detection. This underscores the critical role of rational probe design in developing nucleic acid biosensors capable of robust and accurate performance in practical applications.

Table 4. A comparative table of different kinds of sensors for *E. coli* detection. Detection ranges and LOD are normalized to molar concentration units (M) for consistency.

Method	Detection Range (M)	LOD (M)	Cost	Practicality	Limitation	Ref
Electrochemical DNA sensor (AuE + AuNPs + Cht-Au)	10^{-16}-10^{-6}	10^{-16}	Moderate	High sensitivity, label free detection	Requires electrode modification; lab-based instrumentation	53
Electrochemical DNA sensor (AuNPs+hollow silica particles)	10^{-22}-10^{-17}	1.95×10^{-27}	Moderate	High sensitivity, label free detection	Very complex fabrication; practical use not yet shown	54
Surface enhanced fluorescence (Au@Agnanorods)	10^{-17}-10^{-11}	3.33×10^{-18}	High	Very high sensitivity, specific detection	Complex probe design (Cy3-labeled ssDNA + stem-loop) Costly nanorod synthesis Requires fluorescence instrumentation No real-sample validation	55

Surface Plasmon Resonance (SPR)	10^{-10}-10^{-7}	10^{-11}	High	Label-free, relatively short detection time, high specificity	Requires expensive SPR system; not portable	56
Colorimetric (Gold nanoparticle)	N/A	~ 10^{-7}	Very low	Direct detection of unamplified DNA, food matrix validation	Moderate sensitivity: incubation step needed	57
Electrochemical (DNA-wrapped MWCNTs)	N/A	1.67×10^{-8}	Moderate	Good sensitivity and selectivity; disposable electrodes	Requires PCR amplification; sensitivity lower than SPR/SEF	58
Fluorescent photoluminescent (C-dots)	5×10^{-14} - 2.5×10^{-13}	38.36×10^{-15}	Low	Cost-effective, highly sensitive; simple readout		This work.

Table 4 presents a comparative analysis of representative DNA biosensing strategies for *E. coli*, highlighting that each approach offers distinct advantages and limitations depending on application requirements. Concentration and LOD values have been converted to molar unit (M) to allow for a consistent comparison across different sensors. Conventional electrochemical sensors, including those based on Au-modified electrodes or hollow silica particles, provide high sensitivity, with reported detection limits reaching the femtomolar or sub-femtomolar range, and enable label-free detection. However, their reliance on complex electrode fabrication and sophisticated instrumentation often limits their practicality for field deployment.

Surface-enhanced fluorescence (SEF) and surface plasmon resonance (SPR) systems achieve some of the lowest reported detection limits (3.33×10^{-18} M and 0.01 nM, respectively) while also providing high specificity. Unfortunately, their reliance on expensive materials (e.g., Au@Ag nanorods), multistep probe designs, and high-cost optical equipment limits their accessibility primarily to well-equipped laboratories. In contrast, colorimetric assays employing gold nanoparticles offer a cost-effective, visually interpretable alternative, demonstrating effective detection in real food samples. However, they generally exhibit lower sensitivity and often require additional incubation steps. Similarly, DNA-wrapped MWCNT-based electrochemical sensors provide good selectivity and disposable formats but still depend on prior PCR amplification and show moderate sensitivity compared to optical techniques.

In this context, the carbon dot-based fluorescence biosensor developed in this study offers a balanced combination of sensitivity, simplicity, and cost-effectiveness. The sensor achieves a detection limit of 38.36 fM with a linear detection range of 50-250 fM, while remaining rapid, label-free, and operable with minimal instrumentation. These features substantially reduce both technical complexity and cost compared with SEF or SPR systems. Moreover, the straightforward

fabrication process and uncomplicated fluorescence readout enhance the sensor's potential for practical deployment in pathogen monitoring, environmental analysis, and point-of-care diagnostics, underscoring the promise of carbon-based nanomaterials in next-generation biosensing platforms.

In summary, this study introduces a carbon-dot-based biosensor with high sensitivity and selectivity for bacterial DNA detection. The NH_2-BL21 probe plays a critical role in enhancing specificity and signal stability, while the favorable optical properties and surface functionalization of the C-dots enable efficient target recognition and reliable signal transduction. Nevertheless, the absence of validation in real biological or environmental samples limits assessment of performance in complex matrices. Future work should therefore focus on evaluating the biosensor under realistic conditions to further establish its robustness and practical applicability in diagnostics, environmental monitoring, and related biosensing applications.

Conclusion

This study presents the development of a fluorescence DNA biosensor that employs hydrothermally synthesized carbon dots for the sensitive and selective detection of *E. coli* DNA. The C-dots were characterized using FTIR, EDX, XRD, and FE-SEM techniques, confirming the successful synthesis, effective surface functionalization, and consistent nanoscale morphology of the C-dots. The incorporation of the amino-modified NH_2-BL21 probe significantly enhanced target recognition, demonstrating a strong correlation between *E. coli* DNA concentration and fluorescence intensity. The biosensor exhibited an impressive detection range of 50 to 250 fM, achieving an exceptionally low detection limit of 38.36 fM, along with a recovery rate of 87.06 - 113.57%, indicating high analytical accuracy. Over a four-week period, the biosensor exhibited good stability, with only minor signal reductions and no statistically significant differences

observed. Additionally, it showed minimal cross-reactivity with non-target sequences, confirming its high specificity. Recovery experiments in real water samples confirmed that the C-dot biosensor provides reliable detection of both genomic and synthetic *E. coli* DNA, with minimal interference in drinking and tap water (recoveries 95-126% and 93-119%). Even in complex matrices like lake water, the sensor maintained acceptable accuracy (68-119%). These significant findings underscore the potential of C-dot-based fluorescence biosensors as reliable, accurate, and efficient tools for the rapid detection of *E. coli* DNA, with applications in healthcare, environmental monitoring, and food safety. Future research should focus on investigating the feasibility of multiplexed detection of multiple pathogens.

Funding

This work was supported by VLIR-UOS under grant number VN2025SIN484A101, awarded to Michael Kraft and Mai Thi Tran.

References

1 Basavaraju, M. & Gunashree, B. Escherichia coli: an overview of main characteristics. *Escherichia coli-Old and New Insights* (2022).

2 Sun, H. *et al.* Regulation of flagellar motility and biosynthesis in enterohemorrhagic Escherichia coli O157: H7. *Gut Microbes* **14**, 2110822 (2022).

3 Mare, A. D. *et al.* Enteropathogenic Escherichia coli—A summary of the literature. *Gastroenterology Insights* **12**, 28-40 (2021).

4 Zhou, Y. *et al.* Urinary tract infections caused by uropathogenic Escherichia coli: mechanisms of infection and treatment options. *International journal of molecular sciences* **24**, 10537 (2023).

5 Loos, S. *et al.* Hemoconcentration and predictors in Shiga toxin-producing E. coli-hemolytic uremic syndrome (STEC-HUS). *Pediatric Nephrology* **36**, 3777-3783 (2021).

6 Enciso-Martínez, Y. *et al.* Relevance of tracking the diversity of Escherichia coli pathotypes to reinforce food safety. *International Journal of Food Microbiology* **374**, 109736 (2022).

7 Rani, A., Ravindran, V. B., Surapaneni, A., Mantri, N. & Ball, A. S. Trends in point-of-care diagnosis for Escherichia coli O157: H7 in food and water. *International Journal of Food Microbiology* **349**, 109233 (2021).

8 Bell, R. L. *et al.* The persistence of bacterial pathogens in surface water and its impact on global food safety. *Pathogens* **10**, 1391 (2021).

9 Meyer, C. T. *et al.* A high-throughput and low-waste viability assay for microbes. *Nature Microbiology* **8**, 2304-2314 (2023). https://doi.org/10.1038/s41564-023-01513-9

10 Papkovsky, D. B. & Kerry, J. P. Oxygen sensor-based respirometry and the landscape of microbial testing methods as applicable to food and beverage matrices. *Sensors* **23**, 4519 (2023).

11 Phillips, S. M. *et al.* Engineered cell line imaging assay differentiates pathogenic from non-pathogenic bacteria. *Pathogens* **11**, 209 (2022).

12 Hariri, S. Detection of Escherichia coli in food samples using culture and polymerase chain reaction methods. *Cureus* **14** (2022).

13 Walker, D. I. *et al.* A highly specific Escherichia coli qPCR and its comparison with existing methods for environmental waters. *Water Res* **126**, 101-110 (2017). https://doi.org/10.1016/j.watres.2017.08.032

14 Heijnen, L. *et al.* Qualitative detection of E. coli in distributed drinking water using real-time reverse transcription PCR targeting 16S rRNA: Validation and practical experiences. *Water Research* **259**, 121843 (2024). https://doi.org/10.1016/j.watres.2024.121843

15 Ramezani, R., Kardoost Parizi, Z., Ghorbanmehr, N. & Mirshafiee, H. Rapid and Simple Detection of Escherichia coli by Loop-Mediated Isothermal Amplification Assay in Urine Specimens. *Avicenna J Med Biotechnol* **10**, 269-272 (2018).

16 Shih, C.-M. *et al.* Paper-based ELISA to rapidly detect Escherichia coli. *Talanta* **145**, 2-5 (2015). https://doi.org/10.1016/j.talanta.2015.07.051

17 Selim, S., Harun-Ur-Rashid, M., Jahan, I. & Mostafa, E. M. Culture-Independent molecular techniques for bacterial detection in bivalves. *Egyptian Journal of Aquatic Research* **50**, 585-600 (2024). https://doi.org/10.1016/j.ejar.2024.11.002

18 Hameed, S., Xie, L. & Ying, Y. Conventional and emerging detection techniques for pathogenic bacteria in food science: A review. *Trends in Food Science & Technology* **81**, 61-73 (2018).

19 Pham, T. N. L., Nguyen, S. H. & Tran, M. T. A comprehensive review of transduction methods of lectin-based biosensors in biomedical applications. *Heliyon* (2024).

20 Nguyen, S. H., Nguyen, V.-N. & Tran, M. T. Dual-channel fluorescent sensors based on chitosan-coated Mn-doped ZnS micromaterials to detect ampicillin. *Scientific Reports* **14**, 10066 (2024). https://doi.org/10.1038/s41598-024-59772-3

21 Nguyen, S. H., Vu, P. K. T. & Tran, M. T. Glucose sensors based on chitosan capped Zns doped Mn nanomaterials. *IEEE Sensors Letters* **7**, 1-4 (2023). https://doi.org/10.1109/LSENS.2023.3240240

22 Nguyen, S. H., Nguyen, V.-N. & Tran, M. T. Ampicillin detection using absorbance biosensors utilizing Mn-doped ZnS capped with chitosan micromaterials. *Heliyon* **10**, e31617 (2024). https://doi.org/10.1016/j.heliyon.2024.e31617

23 Nnachi, R. C. *et al.* Biosensors for rapid detection of bacterial pathogens in water, food and environment. *Environment International* **166**, 107357 (2022). https://doi.org/10.1016/j.envint.2022.107357

24 Naresh, V. & Lee, N. A review on biosensors and recent development of nanostructured materials-enabled biosensors. *Sensors* **21**, 1109 (2021).

25 Jenie, S. N. A. *et al.* Rapid Fluorescence Quenching Detection of Escherichia coli Using Natural Silica-Based Nanoparticles. *Sensors* **21**, 881 (2021).

26 Wang, P. *et al.* A highly sensitive upconversion nanoparticles-WS2 nanosheet sensing platform for Escherichia coli detection. *Sensors and Actuators B: Chemical* **320**, 128434 (2020).

27 Tang, X. *et al.* Recent Advances on Fluorescent Sensors for Detection of Pathogenic Bacteria. *Chemosensors* **13**, 182 (2025).

28 Hoang, C. N. M., Nguyen, S. H. & Tran, M. T. Reduced graphene oxide-based absorbance biosensors for detecting Escherichia coli DNA. *Scientific Reports* **15**, 29548 (2025). https://doi.org/10.1038/s41598-025-14189-4

29 Nguyen, S. H., Nguyen, V.-N. & Tran, M. T. Bacillus subtilis DNA fluorescent sensors based on hybrid MoS2 nanosheets. *PLOS ONE* **19**, e0297581 (2024). https://doi.org/10.1371/journal.pone.0297581

30 Ji, C., Zhou, Y., Leblanc, R. & Peng, Z. Recent Developments of Carbon Dots in Biosensing: A Review. *ACS sensors* (2020). https://doi.org/10.1021/acssensors.0c01556

31 Wang, F.-T., Wang, L., Xu, J., Huang, K.-J. & Wu, X. Synthesis and modification of carbon dots for advanced biosensing application. *The Analyst* (2021). https://doi.org/10.1039/d1an00466b

32 Wang, B. *et al.* Carbon Dots in Bioimaging, Biosensing and Therapeutics: A Comprehensive Review. *Small Science* **2** (2022). https://doi.org/10.1002/smsc.202200012

33 Pourmadadi, M. *et al.* Properties and application of carbon quantum dots (CQDs) in biosensors for disease detection: A comprehensive review. *Journal of Drug Delivery Science and Technology* (2023). https://doi.org/10.1016/j.jddst.2023.104156

34 Chandra, S., Chowdhuri, A. R., Mahto, T. K., Samui, A. & Sahu, S. k. One-step synthesis of amikacin modified fluorescent carbon dots for the detection of Gram-negative bacteria like Escherichia coli. *RSC Advances* **6**, 72471-72478 (2016). https://doi.org/10.1039/C6RA15778E

35 Mandal, T. K. & Parvin, N. Rapid Detection of Bacteria by Carbon Quantum Dots. *Journal of Biomedical Nanotechnology* **7**, 846-848 (2011). https://doi.org/10.1166/jbn.2011.1344

36 Saad, S. M. *et al.* A carbon dots based fluorescence sensing for the determination of Escherichia coli O157:H7. *Measurement* **160**, 107845 (2020). https://doi.org/10.1016/j.measurement.2020.107845

37 Xu, P. *et al.* Whole-genome detection using multivalent DNA-coated colloids. *Proc Natl Acad Sci U S A* **120**, e2305995120 (2023). https://doi.org/10.1073/pnas.2305995120

38 Curk, T. *et al.* Computational design of probes to detect bacterial genomes by multivalent binding. *Proceedings of the National Academy of Sciences* **117**, 8719-8726 (2020). https://doi.org/10.1073/pnas.1918274117

39 Behzadi, P., Najafi, A., Behzadi, E. & Ranjbar, R. Microarray long oligo probe designing for Escherichia coli: an in-silico DNA marker extraction. *Cent European J Urol* **69**, 105-111 (2016). https://doi.org/10.5173/ceju.2016.654

40 Garcia, A. *et al.* Quantification of human enteric viruses as alternative indicators of fecal pollution to evaluate wastewater treatment processes. *PeerJ* **10**, e12957 (2022).

41 Chaghaghazardi, M. *et al.* Nitrogen and sulfur co-doped carbon quantum dots fluorescence quenching assay for detection of mercury (II). *Spectrochimica Acta Part A: Molecular and Biomolecular Spectroscopy* **293**, 122448 (2023). https://doi.org/10.1016/j.saa.2023.122448

42 Zhang, X. *et al.* Nitrogen and sulfur co-doped carbon dots with bright fluorescence for intracellular detection of iron ion and thiol. *Journal of colloid and interface science* **611**, 255-264 (2021). https://doi.org/10.1016/j.jcis.2021.12.069

43 Zhou, W. *et al.* Towards efficient dual-emissive carbon dots through sulfur and nitrogen co-doped. *Journal of Materials Chemistry C* **5**, 8014-8021 (2017). https://doi.org/10.1039/C7TC01819C

44 Qiu, D. *et al.* Sulfur-Doped Carbon for Potassium-Ion Battery Anode: Insight into the Doping and Potassium Storage Mechanism of Sulfur. *ACS nano* **16 12**, 21443-21451 (2022). https://doi.org/10.1021/acsnano.2c09845

45 Zhang, H. *et al.* Evolution characteristics of products retorted from Gonghe oil shale based on TG-FTIR and Py-GC/MS. *Thermochimica Acta* **716**, 179325 (2022). https://doi.org/10.1016/j.tca.2022.179325

46 Ragab, M., Deef-Allah, E. & Abdelrahman, M. FTIR Characterization of Asphalt SARA Fractions in Response to Rubber Modification. *Applied Sciences* **15**, 8062 (2025).

47 Nandiyanto, A. B. D., Oktiani, R. & Ragadhita, R. How to read and interpret FTIR spectroscope of organic material. *Indonesian Journal of Science and Technology* **4**, 97-118 (2019).

48 Patil, R. M., Raj R, A., Mondal, S., Bhave, T. & Murthy, A. V. R. An analytical disquisition on the nonlinear optical responses of carbon quantum dots engineered by diverse synthesis methodologies. *Nano Trends* **9**, 100081 (2025). https://doi.org/10.1016/j.nwnano.2025.100081

49 Johny, A., Pinto da Silva, L., Pereira, C. & Silva, J. *Sustainability Assessment of Highly Fluorescent Carbon Dots Derived from Eucalyptus Leaves*. (2023).

50 Lesiak, B. *et al.* Chemical and structural properties of reduced graphene oxide—dependence on the reducing agent. *Journal of Materials Science* **56**, 3738-3754 (2020). https://doi.org/10.1007/s10853-020-05461-1

51 Yang, Z. & Sun, Y. Interlayer spacing of multilayer graphene oxide: Influences of oxygen-containing group density, thickness, temperature and strain. *Applied Surface Science* **529**, 147075 (2020). https://doi.org/10.1016/j.apsusc.2020.147075

52 Penkova, N. A., Sharapov, M. G. & Penkov, N. V. Hydration Shells of DNA from the Point of View of Terahertz Time-Domain Spectroscopy. *International Journal of Molecular Sciences* **22**, 11089 (2021).

53 Wasiewska, L. A. *et al.* Highly sensitive electrochemical sensor for the detection of Shiga toxin-producing E. coli (STEC) using interdigitated micro-electrodes selectively modified with a chitosan-gold nanocomposite. *Electrochimica Acta* **426**, 140748 (2022). https://doi.org/10.1016/j.electacta.2022.140748

54 Yuhana Ariffin, E., Heng, L. Y., Tan, L. L., Abd Karim, N. H. & Hasbullah, S. A. A highly sensitive impedimetric DNA biosensor based on hollow silica microspheres for label-free determination of E. coli. *Sensors* **20**, 1279 (2020).

55 Sun, J. *et al.* DNA biosensor based on fluorescence detection of E. coli O157:H7 by Au@Ag nanorods. *Biosensors and Bioelectronics* **70**, 239-245 (2015). https://doi.org/10.1016/j.bios.2015.03.009

56 Wang, J. *et al.* Rapid label-free identification of mixed bacterial infections by surface plasmon resonance. *Journal of Translational Medicine* **9**, 85 (2011).

57 Dester, E., Kao, K. & Alocilja, E. C. Detection of unamplified E. coli O157 DNA extracted from large food samples using a gold nanoparticle colorimetric biosensor. *Biosensors* **12**, 274 (2022).

58 Ozkan-Ariksoysal, D. *et al.* DNA-wrapped multi-walled carbon nanotube modified electrochemical biosensor for the detection of Escherichia coli from real samples. *Talanta* **166**, 27-35 (2017). https://doi.org/10.1016/j.talanta.2017.01.005

Acknowledgement

The authors gratefully acknowledge Dr. Quynh Le of VinUniversity for his generosity in allowing us to use the SpectraPro HRS-300 spectrophotometer.

Author contributions statement

Chau Nguyen Minh Hoang: Formal analysis, Validation, Methodology, Data curation, Visualization, Original writing. **Son Hai Nguyen:** Conceptualization, Resources, Formal analysis, Methodology, Administration, Validation, Methodology, Visualization, Original writing, and editing. **Michael Kraft:** Methodology, Validation, Reviewing and editing, Funding acquisition. **Mai Thi Tran:** Methodology, Investigation, Formal analysis, Validation, Visualization, Funding acquisition, Original writing, and editing.

Data and materials availability

The datasets used and analyzed during the current study are available from the corresponding author upon reasonable request.